Title

Structural Change Can Be Detected in Advanced-Glaucoma Eyes.

Journal

Investigative ophthalmology & visual science, 57(9)

ISSN

0146-0404

Authors

Belghith, Akram
Medeiros, Felipe A
Bowd, Christopher
et al.

Publication Date

2016-07-01

DOI

10.1167/iovs.15-18929

Peer reviewed

Special Issue

Structural Change Can Be Detected in Advanced-Glaucoma Eyes

Akram Belghith,[1] Felipe A. Medeiros,[1] Christopher Bowd,[1] Jeffrey M. Liebmann,[2] Christopher A. Girkin,[3] Robert N. Weinreb,[1] and Linda M. Zangwill[1]

[1]Shiley Eye Institute, Hamilton Glaucoma Center, University of California, San Diego, La Jolla, California, United States
[2]Harkness Eye Institute, Columbia University, New York, New York, United States
[3]Ophthalmology, University of Alabama, Birmingham, Alabama, United States

Correspondence: Linda M. Zangwill, Department of Ophthalmology – 0946, University of California, San Diego, 9500 Gilman Drive, La Jolla, CA 92093, USA; lzangwill@ucsd.edu.

Submitted: December 14, 2015
Accepted: June 1, 2016

Citation: Belghith A, Medeiros FA, Bowd C, et al. Structural change can be detected in advanced-glaucoma eyes. *Invest Ophthalmol Vis Sci*. 2016;57:OCT511–OCT518. DOI:10.1167/iovs.15-18929

Purpose. To compare spectral-domain optical coherence tomography (SD-OCT) standard structural measures and a new three-dimensional (3D) volume optic nerve head (ONH) change detection method for detecting change over time in severely advanced-glaucoma (open-angle glaucoma [OAG]) patients.

Methods. Thirty-five eyes of 35 patients with very advanced glaucoma (defined as a visual field mean deviation < -21 dB) and 46 eyes of 30 healthy subjects to estimate aging changes were included. Circumpapillary retinal fiber layer thickness (cpRNFL), minimum rim width (MRW), and macular retinal ganglion cell–inner plexiform layer (GCIPL) thicknesses were measured using the San Diego Automated Layer Segmentation Algorithm (SALSA). Progression was defined as structural loss faster than 95th percentile of healthy eyes. Three-dimensional volume ONH change was estimated using the Bayesian-kernel detection scheme (BKDS), which does not require extensive retinal layer segmentation.

Results. The number of progressing glaucoma eyes identified was highest for 3D volume BKDS (13, 37%), followed by GCPIL (11, 31%), cpRNFL (4, 11%), and MRW (2, 6%). In advanced-OAG eyes, only the mean rate of GCIPL change reached statistical significance, -0.18 μm/y ($P = 0.02$); the mean rates of cpRNFL and MRW change were not statistically different from zero. In healthy eyes, the mean rates of cpRNFL, MRW, and GCIPL change were significantly different from zero. (all $P < 0.001$).

Conclusions. Ganglion cell–inner plexiform layer and 3D volume BKDS show promise for identifying change in severely advanced glaucoma. These results suggest that structural change can be detected in very advanced disease. Longer follow-up is needed to determine whether changes identified are false positives or true progression.

Keywords: advanced glaucoma, structural change, 3D change detection, rate of change

Primary open-angle glaucoma (OAG) is often an asymptomatic disease at its most treatable stages and can therefore be quite advanced at the time of initial detection, particularly in high-risk populations. An estimated 10% to 39% of patients present with advanced glaucoma (OAG), and many are asymptomatic at the time of diagnosis.[1–3] Moreover, as the population ages and life expectancy increases, a larger proportion of patients will develop advanced disease. Advanced-OAG patients are, however, at the highest risk of becoming functionally impaired due to the disease and are the costliest to treat.[4–6] Clinicians need to know whether the patient is stable on the current therapy or whether the patient is progressing and therapy needs to be intensified.

Unfortunately, there are currently no accepted standards for which tests are most effective for detection of progressive glaucoma in advanced OAG. Assessment of glaucoma progression in early stages of the disease is usually performed by detecting change over time in structural and functional measurements such as circumpapillary retinal nerve fiber layer thickness (cpRNFL), optic nerve head (ONH) neuroretinal minimum rim width (MRW), retinal ganglion cell–inner plexiform layer (GCIPL) thickness, and visual field mean deviation (VF MD).[7–9] However, monitoring advanced OAG using standard structural and functional testing is extremely difficult for the treating clinician since both standard structural and functional tests that usually guide treatment decisions are of diminished value. This is because standard structural measures have a limited dynamic range as they thin with advanced OAG, and visual field (VF) test points are more variable in advanced disease.[10–16] Complicating matters further, recent reimbursement criteria in the United States have limited the use of imaging in advanced OAG[17] because VF testing is considered more diagnostic in advanced disease.

Despite advances in spectral-domain optical coherence tomography (SD-OCT) imaging, few studies have evaluated whether SD-OCT can detect structural change in advanced disease. Evidence suggests that in advanced OAG, the papillomacular bundle is more resistant to glaucomatous damage and shows better agreement with VF progression than cpRNFL and thus may be used to monitor glaucomatous change in late stages of the disease.[7,8]

Recently, we proposed a new glaucoma change detection method (Bayesian-kernel detection scheme [BKDS]) that utilizes the whole three-dimensional (3D) SD-OCT ONH and

Investigative Ophthalmology & Visual Science

does not require extensive retinal layer segmentation.[18,19] In early- to moderate-glaucoma eyes with progressing VF damage, while maintaining high specificity the BKDS method had higher sensitivity for detecting progression than cpRNFL.[18,19] This method also has the advantage that it detects 3D change in a region of interest, which can include deeper layers such as the lamina cribrosa. Reports suggest that in eyes with advanced glaucoma, the lamina cribrosa changes its shape by developing a W-shaped configuration.[20] Others have reported that the lamina cribrosa is cupped and excavated beneath the scleral canal rim in advanced-OAG eyes.[21]

The purpose of this study was to determine whether MRW, cpRNFL, and GCIPL thinning can be detected in very advanced OAG eyes and to compare the number of progressing OAG eyes using these measurements with a new 3D ONH whole-volume change detection method, BKDS.

Methods

Subjects

Patients with primary OAG and healthy subjects included in this study were recruited from the Diagnostic Innovations in Glaucoma Study (DIGS) and African Descent and Glaucoma Evaluation Study (ADAGES). The multicenter ADAGES includes participants from the Hamilton Glaucoma Center at the Department of Ophthalmology, University of California-San Diego; the New York Eye and Ear Infirmary; and the Department of Ophthalmology, University of Alabama at Birmingham. The Diagnostic Innovations in Glaucoma Study includes participants recruited at the University of California-San Diego. All the methods adhered to the tenets of the Declaration of Helsinki and to the Health Insurance Portability and Accountability Act. The institutional review boards at the University of California-San Diego, New York Eye and Ear Infirmary, and University of Alabama at Birmingham approved the methods. All participants of the study gave written informed consent. The African Descent and Glaucoma Evaluation Study and DIGS are registered as cohort clinical trials (http://www.clinicaltrials.gov, identifiers NCT00221923 and NCT00221897, September 14, 2005).

Methodological details of DIGS and ADAGES have been described previously.[22] In brief, for glaucoma subjects, inclusion criteria were 20/40 or better best-corrected visual acuity at baseline, spherical refraction within ±5.0 diopters (D), cylinder correction within ±3.0 D, open angles on gonioscopy, and at least two consecutive and reliable standard automated perimetry VF examinations with either a pattern standard deviation (PSD) or a glaucoma hemifield test (GHT) result outside the 99% normal limits. Exclusion criteria were eyes with coexisting retinal disease and eyes with non-glaucomatous optic neuropathy.

For healthy subjects, inclusion criteria were 20/40 or better best-corrected visual acuity, spherical refraction within ±5.0 D, cylinder correction within ±3.0 D, IOP $<$ 22 mm Hg with no history of elevated IOP, and at least two reliable normal VFs, defined as a PSD within 95% confidence limits and a GHT result within normal limits.

All subjects underwent an annual comprehensive ophthalmologic examination including review of medical history, best-corrected visual acuity, slit-lamp biomicroscopy, dilated funduscopic examination, and stereoscopic optic disc photography. Semiannual examination included intraocular pressure (IOP), SD-OCT imaging (SD-OCT circular scan, SD-OCT ONH cube scan, SD-OCT ONH radial scan, and SD-OCT macular cube scan), and VF testing.

In this report, we included three groups of participants. The first group was composed of 35 eyes of 35 advanced-glaucoma patients (VF MD ≤ -21 dB) followed for an average of 3.5 ± 0.9 years. All eyes were followed at approximately 6-month intervals with VF and OCT testing and were required to have a minimum of three VFs and three OCTs during follow-up for inclusion in this study (number of tests ranged from three to eight).

The stable glaucoma group of consisted of 50 eyes from 27 early-, moderate-, and advanced-glaucoma patients with five serial OCT exams imaged every week for 5 weeks. We assume that in this short follow-up period, glaucoma changes are not likely to occur. These stable glaucoma eyes were used to train the BKDS ONH volume change method to reduce the likelihood that changes due to measurement variability would be classified as progression due to glaucoma.

A third group of 46 eyes from 30 healthy subjects followed for an average of 2.8 ± 0.4 years was used to estimate the aging effects. All eyes were followed at approximately 6-month intervals with VF and OCT testing and had an average of six tests acquired during follow-up (test range was 4–10). Healthy participants were recruited from the general population through advertisement, from referring practices, and from the staff and employees from the Shiley Eye Institute, University of California, San Diego.

Imaging

Each subject was required to have at least one good-quality Spectralis SD-OCT (Heidelberg Engineering Inc., Heidelberg, Germany) circular scan, SD-OCT ONH cube scan, SD-OCT ONH radial scan, and SD-OCT macular cube scan acquired on the same day. Spectralis OCT uses a dual-beam SD OCT, a confocal laser-scanning ophthalmoscope with a wavelength of 870 nm, and an infrared reference image to obtain images of ocular microstructures. The instrument has an acquisition rate of 40,000 A-scans per second. Spectralis OCT incorporates a real-time eye-tracking system that couples confocal laser-scanning ophthalmoscope and SD OCT scanners to adjust for eye movements and to ensure that the same location of the retina is scanned over time. The image acquisition protocols included (1) high-resolution RNFL circle scan, which consists of 1536 A-scan points from a 3.45-mm circle centered on the optic disc, (2) high-resolution cube scan centered on the optic disc (73 B-scans with 768 A-scans each), (3) enhanced depth imaging (EDI) scan centered on the optic disc (48 B-scans with 1024 A-scans each), and (4) high-resolution cubic scan centered on the fovea (73 B-scans with 768 A-scans each). Quality assessment of OCT scans was evaluated by Imaging Data Evaluation and Assessment (IDEA) Center experienced examiners masked to the subject's results of the other tests.

San Diego Automated Layer Segmentation Algorithm (SALSA)

Raw 3D SD-OCT images were exported to a numerical computing language (MATLAB; MathWorks, Natick, MA, USA). The San Diego Automated Layer Segmentation Algorithm (SALSA) was used to automatically segment (1) the Bruch's membrane opening (BMO) and the internal limiting membrane (ILM) on each ONH radial scan to calculate the MRW defined as the shortest distance from BMO to ILM, and (2) the macular GCIPL from the macular cube scan. The Spectralis built-in segmentation algorithm was used to segment the cpRNFL from the circular scan. Details of the SALSA have been described previously.[23–25] Briefly, we assumed that each B-scan consists of several interretinal layers (e.g., the Bruch's membrane [BM] layer, the retinal nerve fiber layer [RNFL]). Because the

Investigative Ophthalmology & Visual Science

Table 1. Baseline Characteristics of Study Subjects

	Healthy	Stable	Advanced Glaucoma	ANOVA *P* Value
Number of eyes	46	50	35	
Sex, % female	55	61	57	0.74
Age at baseline, y	59 ± 8.7	68 ± 7.1	67 ± 11.3	<0.001
Follow-up length, y	2.8 ± 0.4	5 wk	3.5 ± 0.9	<0.001
Axial length, mm	23.9 ± 1.6	24.2 ± 2.1	24.3 ± 2.4	0.65
Heidelberg Retina Tomograph optic disc area, mm^2	2.17 ± 0.44	2.19 ± 0.41	2.16 ± 0.47	0.57
Mean deviation, dB (range)	1.02 (−1.2 to 2.3)	−6.3 (−11.4 to −1.3)	−28 (−33 to −21)	<0.001

All values are mean (±SD) and ANOVA results with post hoc Tukey test *P* values reported representing the differences between healthy and glaucoma eyes.

interretinal layers have different thicknesses, each layer can be defined by a curve modeling its skeleton and a filter or set of filters modeling its thickness. To segment the different layers, it is sufficient to estimate their skeletons and the hyperparameters of the filters. In this study, we are interested only in the segmentation of the BM, ILM layers in the ONH scans, and RNFL and IPL layers in the macular scans. In order to build connected skeletons, we considered an object-oriented approach rather than the voxel-oriented approach.[26] Therefore, short segments (20 voxels in our case) are added to or deleted from the current configuration depending on their state (connected or not). Note that shorter segments have been considered in the termination of the skeletons for better estimation accuracy. The estimation of the model parameters and hyperparameters are addressed using a Monte Carlo Markov chain.[27] For the BMO identification, once we estimated the BM layer separately in each of the 48 B-scans, we utilized the whole 3D volume to estimate the BMO points to take into account the planarity of the BMO points. Our aim is to properly integrate the elliptical shape of the BMO curve and to rely only on the reliable BMO points in the estimation scheme. Note that our aim is not to fit an ellipse to the data but to use the elliptical shape as a Bayesian "prior" shape to estimate the curve that best represents the data. An elegant way to address this task is to use the inverse artificial neural network ANN-PCA to model the elliptical shape of the BMO curve.[28]

Bayesian-Kernel Detection Scheme

The Bayesian-kernel detection scheme is a Bayesian-based approach that uses change in the 3D ONH volume scans to classify an eye as "nonprogressing" or "progressing." Details of the BKDS have been described previously.[18,19] In brief, raw 3D SD-OCT ONH cube scans were exported to a numerical computing language (MATLAB, MathWorks). The Bayesian-kernel detection scheme was used to estimate glaucoma progression from ONH cube scans. We formulated the detection of glaucomatous change between baseline image and follow-up images as a missing data problem. Markov random field model (MRF) prior was used to model the spatial dependency of changed voxels. Once the change detection map was estimated, we used a kernel-based classifier for glaucoma progression detection. As prior knowledge or an agreed-upon "gold standard" for detection of progression in advanced glaucoma is not available, we used a one-class classifier trained only on the nonprogressing 50 stable glaucoma eyes and 36 healthy eyes. We utilized a support vector data description (SVDD) classifier.[19] The SVDD enables us to distinguish between targets (nonprogressing eyes) and outliers (progressing eyes) by defining a closed boundary around the target data. As done previously,[29] we included two features as input for the SVDD based on a glaucoma-related region of interest of the baseline image that generally consists of the RNFL, neuoretinal rim, and prelamina tissue of the ONH identified using SALSA. Follow-up images were automatically registered by the instrument to the baseline image to detect change over time at specific locations in the region of interest. Please note that retinal layer segmentation of the follow-up images is not required. The two features identified in the region of interest are the number of voxels detected as "changed," and the ratio image intensity between the baseline and follow-up scans of changed voxels.

Definition of Progression

An eye was defined as progressing if (1) macular GCIPL, MRW, or cRNFL loss was significantly ($P < 0.05$) different from zero and faster than the 5th percentile of the healthy group or (2) 3D ONH volume BKDS change was classified as progressing utilizing both the healthy group and stable glaucoma group in the one-class SVDD classification method.

Statistical Analysis

Descriptive statistics were used to compare demographic characteristics by group (healthy and glaucoma subjects). χ^2 tests were used to compare categorical variables, and *t*-tests were used to compare continuous variables. Mixed effects models were used to calculate the mean rates of change (slopes) for global cpRNFL thickness, global MRW thickness, and global macular GCIPL thickness loss from baseline. Models included group (healthy versus glaucoma), time, and the interaction term group × time. *P* values less than 0.05 were considered statistically significant. The model was adjusted for age, and the correlation between eyes was accounted for in the model. Statistical analysis was performed using SAS, Version 9.2 (SAS Institute, Cary, NC, USA).

Results

The study included 35 eyes of 35 glaucoma patients with very advanced glaucoma, 50 eyes from 27 stable glaucoma, and 46 eyes from 30 healthy subjects. A summary of the demographic variables and measurements at baseline of each group is shown

Table 2. Baseline Global cpRNFL, MRW, and Macular GCIPL Measurements by Group

	Healthy	Advanced Glaucoma	*P* Value
cpRNFL, μm	94.3 ± 10.4	56.2 ± 5.11	<0.001
MRW, μm	211.5 ± 59.3	134.6 ± 18.7	<0.001
Macular GCIPL, μm	89.7 ± 7.5	61.4 ± 9.1	<0.001

All values are mean (±SD) and Wilcoxon rank sum test *P* values reported representing the differences between healthy and advanced-glaucoma eyes.

Table 3. Rates of Global cpRNFL, MRW, Macular GCIPL, and VF MD Loss by Group

	Healthy, $n = 46$			Advanced Glaucoma, $n = 35$			
	Mean	(95% CI)	*P* Value	Mean	(95% CI)	*P* Value	*P* Value*
cpRNFL, μm/y	−0.32	(−0.51, −0.14)	<0.001	−0.08	(−0.21, 0.19)	0.39	0.44
MRW, μm/y	−1.41	(−1.45, −1.18)	<0.001	−0.29	(−0.86, 0.73)	0.43	0.58
GCIPL, μm/y	−0.11	(−0.15, −0.01)	<0.001	−0.18	(−0.25, −0.06)	0.02	1.12
VF MD, dB/y	0.07	(−0.19, 0.26)	0.65	0.02	(−0.08, 0.16)	0.47	0.82

CI, confidence interval.
* *P* value evaluates differences in the mean rate of change between healthy and glaucoma eyes.

Table 4. Baseline Global cpRNFL, MRW, Macular GCIPL, and VF MD Measurements by Group

	3D Whole-Volume BKDS Criterion			Macular GCIPL Criterion		
	Nonprogressing, $n = 22$	Progressing, $n = 13$		Nonprogressing, $n = 24$	Progressing, $n = 11$	
	Mean ± SD	Mean ± SD	*P* Value	Mean ± SD	Mean ± SD	*P* Value
cpRNFL, μm	55.7 ± 5.3	56.7 ± 6.4	0.72	54.2 ± 6.4	58.2 ± 7.1	0.39
MRW, μm	133.8 ± 19.5	135.4 ± 21.3	0.84	132.4 ± 21.3	136.8 ± 22.4	0.43
GCIPL, μm	59.1 ± 8.7	63.7 ± 9.5	0.15	59.8 ± 8.2	63 ± 9.8	0.09
VF MD, dB	26.4 ± 2.9	29.6 ± 3.8	0.11	27.7 ± 3.1	28.3 ± 3.4	0.34

All values are mean (±SD) and Wilcoxon rank sum test of the differences between nonprogressing and progressing glaucoma eyes.

Table 5. Rate of Global cpRNFL, MRW, Macular GCIPL, and VF MD Loss by Group

	3D Whole-Volume BKDS Criterion			Macular GCIPL Criterion		
	Nonprogressing, $n = 22$	Progressing, $n = 13$		Nonprogressing, $n = 24$	Progressing, $n = 11$	
	Mean ± SD	Mean ± SD	*P* Value	Mean ± SD	Mean ± SD	*P* Value
cpRNFL, μm/y	−0.07 ± 0.02	−0.09 ± 0.03	0.48	−0.06 ± 0.01	−0.08 ± 0.03	0.37
MRW, μm/y	−0.27 ± 0.07	−0.33 ± −0.11	0.71	−0.28 ± 0.06	−0.32 ± 0.12	0.58
GCIPL, μm/y	−0.11 ± 0.04	−0.24 ± 0.05	0.03	0.1 ± 0.05	0.27 ± 0.05	0.01
VF MD, dB/y	0.02 ± 0.01	0.04 ± 0.02	0.34	0.05 ± 0.02	0.04 ± 0.03	0.20

All values are mean (±SD) and Wilcoxon rank sum test of the differences between nonprogressing and progressing glaucoma eyes.

in Table 1. Glaucoma patients were significantly older ($P < 0.001$) and had worse VF MD ($P < 0.001$) and longer follow-up ($P < 0.001$) than healthy subjects. The advanced-glaucoma and the healthy eye groups were similar with respect to sex ($P = 0.74$), axial length ($P = 0.65$), and disc area ($P = 0.57$).

Structural Rate of Change

Baseline global cpRNFL thickness derived from the circular scan, global MRW thickness derived from the ONH radial scan, and macular GCIPL thickness derived from the entire macular cube SD-OCT scan measurements in healthy and advanced-glaucoma eyes are presented in Table 2. Healthy eyes had thicker baseline cpRNFL, MRW, and macular GCIPL when compared to glaucoma eyes.

Rates of global cpRNFL, MRW, and macular GCIPL thickness loss in healthy and advanced-glaucoma eyes are presented in Figure 1 and Table 3. In healthy eyes, mean rates (*P* value) of cpRNFL, MRW, and macular GCIPL were –0.32 μm/y ($P < 0.001$), –1.41 μm/y ($P < 0.001$), and –0.11 μm/y ($P < 0.001$), respectively. In advanced-glaucoma eyes, the mean rates of cpRNFL, MRW, and macular GCIPL change were –0.08 μm/y ($P = 0.39$), –0.29 μm/y ($P = 0.43$), and –0.18 μm/y ($P < 0.02$), respectively. There was no statistically significant difference between the mean rate of loss of cpRNFL and MRW in advanced-glaucoma eyes and healthy eyes ($P = 0.44$ and $P = 0.58$). The mean rate of macular GCIPL loss tended to be larger in advanced-glaucoma eyes than in healthy eyes, but the difference in mean rates between the two groups was not statistically significant ($P = 0.12$).

Glaucoma Progression Detection

By the structural measurement rate of change criterion, the number of identified progressing glaucoma eyes was 2 (5%) using cpRNFL, 4 (11%) using the MRW, and 11 (31%) using the macular GCIPL. Table 4 presents baseline global cpRNFL, MRW, macular GCIPL, and VF MD measurements by study group; Table 5 presents the mean rates of global cpRNFL, MRW, macular GCIPL, and VF MD loss by study group. No significant

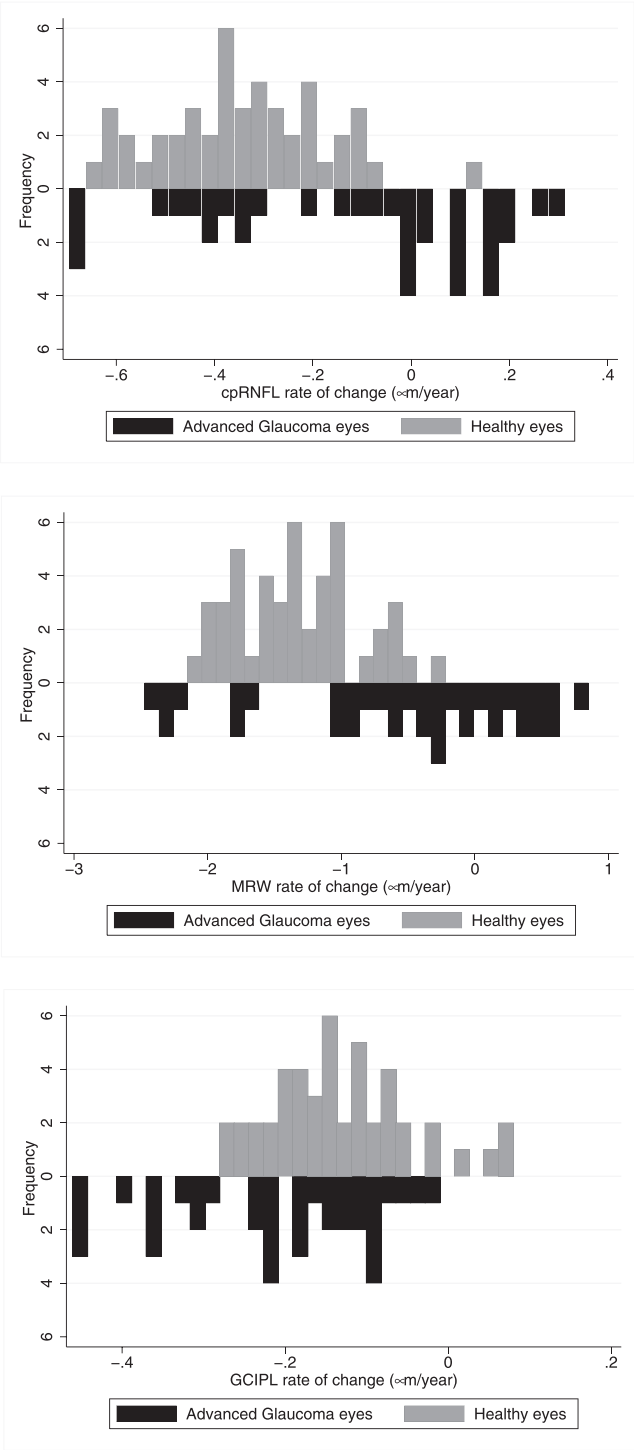

Figure 1. Distribution of the mean rates of change of circumpapillary retinal nerve fiber layer (cpRNFL), minimum rim width (MRW), and macular ganglion cell–inner plexiform layer (GCIPL) thickness in healthy and advanced-glaucoma eyes.

difference was found between the VF MD baseline measurement and MD mean rate of change of the 11 eyes that progressed based on the macular GCIPL criteria and 24 eyes that did not progress ($P = 0.34$, $P = 0.2$, respectively). However, mean macular GCIPL thickness tended to be larger in the 11 eyes that progressed compared to the eyes that did not ($P = 0.09$). There was no significant difference in cpRNFL and MRW thickness and mean rate of change between the 11 progressing eyes based on GCIPL and the eyes that did not progress ($P = 0.39$, $P = 0.43$ and $P = 0.37$, $P = 0.58$, respectively). Figure 2 shows the cpRNFL, MRW, macular GCIPL thickness, and VF of an eye identified as progressing by cpRNFL, MRW, and macular GCIPL. Figure 3 shows the cpRNFL, MRW, macular GCIPL thickness, and VF of an eye with progression detected only by macular GCIPL.

Using the 3D whole-volume BKDS method, the number of progressing glaucoma eyes identified was 13 (31%). Among the 13 progressing eyes detected by the 3D whole-volume BKDS, 7 eyes were also identified by macular GCIPL, 3 eyes by MRW, and 1 eye by cpRNFL. Using the 3D whole-volume BKDS method, no significant difference was found between the VF MD baseline measurement and MD rate of change of the 13 eyes that progressed based on the BKDS and 22 eyes that did not progress ($P = 0.11$, $P = 0.3$, respectively). The GCIPL mean rate of change was significantly faster in BKDS progressing eyes than nonprogressing eyes ($P = 0.03$). There was no significant difference in baseline cpRNFL and MRW thickness and mean rate of change between the 13 BKDS progressing eyes and 22 nonprogressing eyes ($P = 0.72$, $P = 0.84$ and $P = 0.48$ and $P =$ 71, respectively).

Discussion

Our results suggest that even in very advanced glaucoma, structural loss can be detected in some eyes using standard global structural measures. Specifically, macular GCIPL had the highest proportion of eyes with detectable change (31%), followed by MRW (11%) and cpRNFL (4%). In addition, the 3D whole-volume BKDS change method, which does not require extensive retinal layer segmentation, detected change in 37% of eyes. Moreover, only the mean rate of macular GCIPL change reached statistical significance, suggesting that GCIPL changes can be detected even in this group of severely advanced-OAG eyes. In contrast, the mean rates of change in cpRNFL and MRW were not significantly different from zero. The mean rates of change in the healthy eyes were all significantly different from zero, suggesting that aging effects can be detected even in a relatively short follow-up time.

These results are important as detecting change in advanced-OAG eyes is challenging, as the amount of remaining measurable neural tissue is limited. Moreover, determining whether the glaucoma patient is stable or progressing is critical for determining whether the treatment initiated needs to be changed or intensified, as patients with advanced glaucoma are at a high risk of losing remaining vision and becoming functionally impaired or blind from the disease.

This study is unique in that it focused on identification of change in very advanced disease where the usefulness of conventional structural and functional tests that usually guide treatment decisions is reduced (i.e., VF and cpRNFL thickness). While the VF MD is commonly used to classify the glaucoma subject into early, moderate, and advanced disease, it may not accurately reflect the extent of structural loss. For example, one eye with only a focal cpRNFL defect may have the same VF MD value as another eye with a diffuse cpRNFL defect. In the first case it is possible that the RNFL thickness in sectors without the focal defect can still be used to monitor further change, which is less likely the case for the second eye. Therefore, this report can be considered as a proof of concept; if structural change was detectable in this very advanced stage of the disease using existing and novel methods for change detection, then structural change is also likely to be detectable in eyes with less advanced disease.

Investigative Ophthalmology & Visual Science

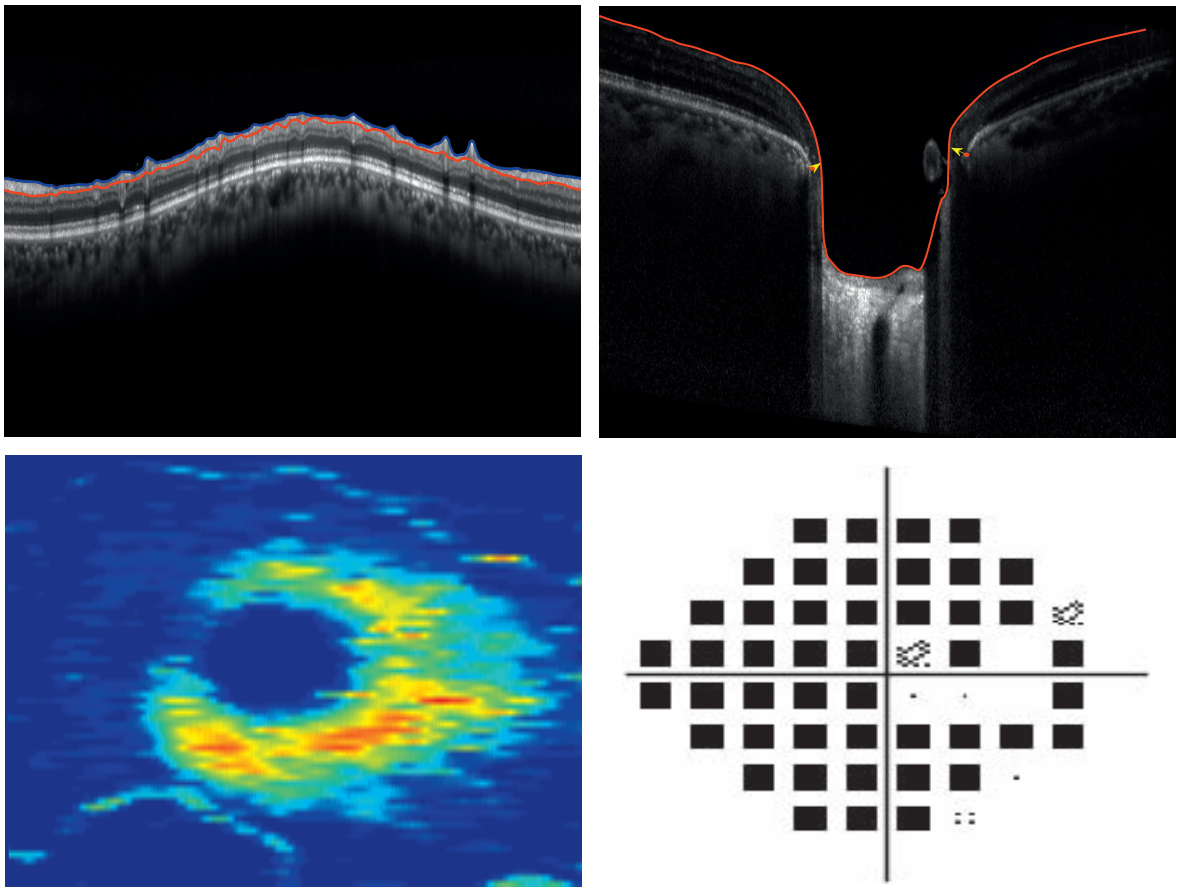

Figure 2. *Top row*: circumpapillary retinal nerve fiber layer (cpRNFL), minimum rim width (MRW), *Bottom row*: macular ganglion cell–inner plexiform layer (GCIPL) thickness, and 24-2 visual field in one eye detected as glaucoma progressing by cpRNFL, MRW, and macular GCIPL (MD VF = −22.3).

Recent advances in SD-OCT technology have improved image resolution, made it possible to measure retina layer thickness and ONH parameters, and allowed the imaging of deeper retinal structures such as the choroid and the lamina cribrosa.[30] For these reasons, SD-OCT has been widely adopted clinically to objectively assess small changes in the retina. In the current study, we evaluated the rate of change of cpRNFL thickness, MRW, and macular GCIPL in advanced-glaucoma eyes and compared the number of progressing glaucoma eyes using these measurements to a new 3D optic ONH whole-volume change detection method, BKDS, that does not require retinal layer segmentation.

Retinal layer segmentation is particularly challenging in eyes with advanced disease as the layers are thin, and results are more variable than in eyes with less severe glaucoma. This issue is of particular importance for cpRNFL segmentation, as the presence of large blood vessels can adversely affect segmentation of the thin cpRNFL in advanced disease.[31] Similarly, differentiating between the ganglion cell layer (GCL) and IPL is particularly challenging when the layers are thin, as in advanced OAG. For this reason, we analyzed the macular GCIPL and not the GCL as a separate layer. The SALSA and Spectralis instrument–based retinal layer segmentation of eyes included in this study were manually checked and did not have segmentation failures of the macular GCIPL, MRW, or cpRNFL.

There are several possible reasons why we found faster cpRNFL and MRW change in healthy subjects than in advanced-glaucoma patients. First, healthy subjects were younger than OAG patients and had thicker baseline values. In addition, cpRNFL and MRW atrophy is already extensive in patients with advanced glaucoma. Therefore, identification of cpRNFL and MRW changes is more challenging at later stages of glaucoma when the layers have already thinned.

The 3D whole-volume BKDS offers several advantages compared to retinal structural- and thickness-based methods. First, the 3D whole-volume BKDS does not require accurate segmentation of each retinal layer on each scan. Rather, a glaucoma-based region of interest, generally consisting of RNFL, neuroretinal rim, and prelamina tissue, is delineated on the baseline scan only. Therefore, measurement variability inherent in retinal layer segmentation algorithms will not adversely affect the ability to detect progression. The BKDS also facilitates the analysis of the entire ONH 3D volume for potential glaucomatous changes that may occur in the region of interest that also includes deeper layers such as prelaminar tissue. Moreover, the use of spatial dependency favors the generation of homogeneous areas, reducing the likelihood of false-positive detection of change. Third, the proposed kernel-based support vector data description (SVDD) method allows the classifier to be trained using only nonprogressing eyes. This is important because there is no generally accepted definition or "gold standard" for detection of progression in advanced glaucoma that can be used to identify progressing eyes for use in training the classifier. It is important to note that we have previously demonstrated the utility of the BKDS for detection of ONH progression in early- to moderate-glaucoma eyes using VF progression as the "gold standard."[18,19] Finally, BKDS can

Investigative Ophthalmology & Visual Science

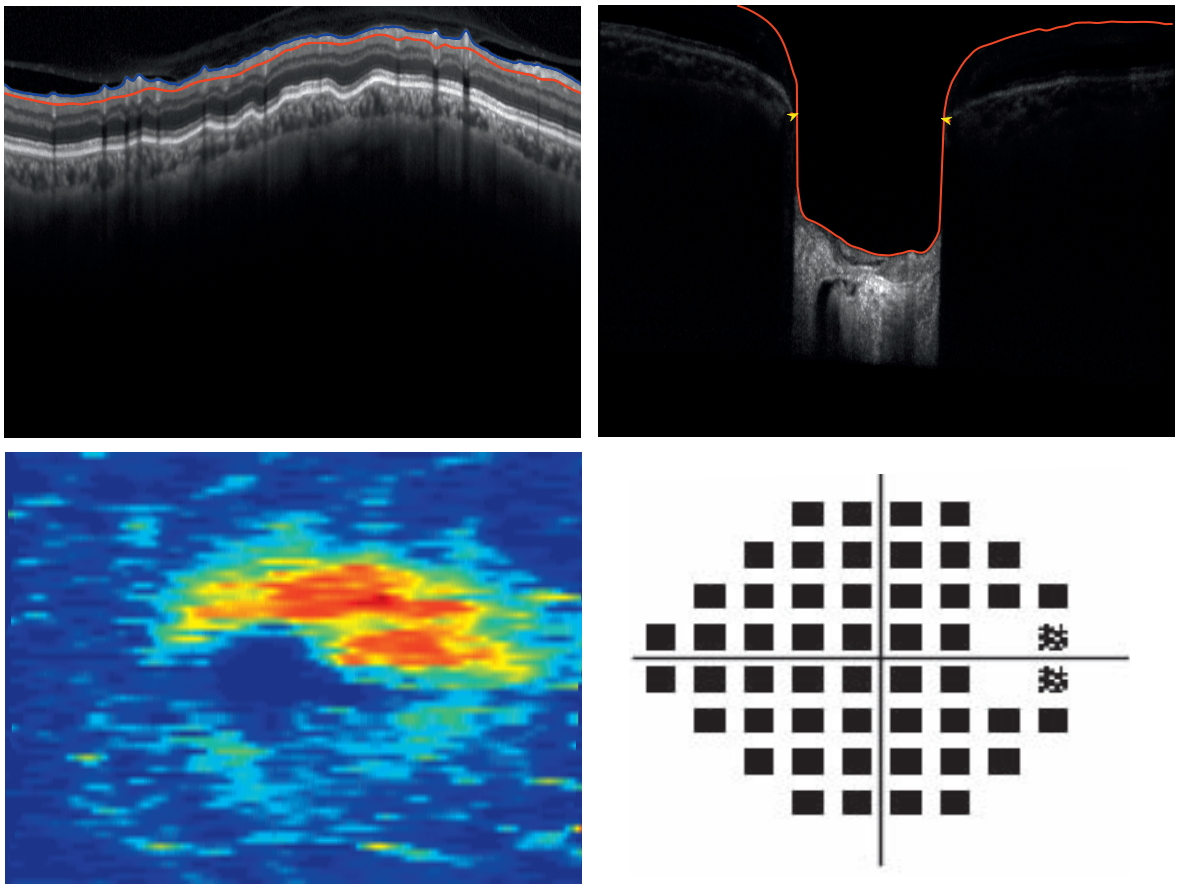

Figure 3. *Top row*: circumpapillary retinal nerve fiber layer (cpRNFL), minimum rim width (MRW), *Bottom row*: macular ganglion cell–inner plexiform layer (GCIPL) thickness, and 24-2 visual field in one eye detected as glaucoma progressing by only macular GCIPL (MD VF = −28.46).

be tailored to specific progression detection tasks. For example, in our previous publications, BKDS was implemented without any retinal layer segmentation.[18] In the current study, a region of interest was defined by segmentation of the baseline images and progression detection limited to the designated region of interest.

There are several limitations to the 3D whole-volume BKDS method that should be noted. One limitation of the proposed method is the inclusion of retinal blood vessels in the change detection map. Although the variation of retinal blood vessels may be compensated for by the classifier, this compensation by the classification algorithm could mask small changes in the RNFL or rim area. Another limitation is the lack of a parameter to assess and quantify the rate of progression, which may be helpful for clinicians to estimate the likelihood that a patient will become functionally impaired in his or her lifetime.[16] Further, it is difficult to assess whether the detected changes are due to glaucomatous changes or other tissue remodeling that is not related to progression of the disease. Nevertheless, while it is unclear if the detected changes are related or not to the glaucoma, it is important for the clinician to evaluate change that is outside normal limits.

Limitations of the current study include the small sample size, relative short follow-up time for both healthy subjects and glaucoma patients, and the limited age range of the healthy subjects. For these reasons, the proportion of progressing eyes and rates of change measured for GCIPL, MRW, and cpRNFL in this specific severely advanced-glaucoma group may not be generalizable to other groups of advanced-glaucoma patients. In addition, without a gold standard definition of progression in advanced disease, it is difficult to determine whether the detected changes are glaucomatous changes or age-related changes, or, as previously mentioned, to tissue remodeling not necessarily related to OAG. We utilized nonprogressing healthy and stable glaucoma eyes in the analysis to reduce the possibility that the changes identified were due to aging or variability of the measurements. Nevertheless, while it is unclear if the detected changes are related or not to the glaucoma, characterizing these changes may improve our understanding of the pathophysiology of glaucoma or age-related changes in these eyes with advanced disease. Another limitation is the use of the global measurements to assess the rate of change of cpRNFL, MRW, and GCIPL. While using global measurements results in reduced variability compared to sectoral measurements, in advanced OAG, they may underestimate the changes at locations where there is a region in which neural tissue remains intact. The development of automated methods to detect the remaining neural tissue may be helpful to assess more accurately regions of interest for monitoring the structural rate of change.

In conclusion, our results suggest that even in very advanced disease, structural change can be detected, and that monitoring macular GCIPL and 3D whole-volume BKDS change shows promise for identifying progression in advanced glaucoma. However, a larger sample of advanced-glaucoma patients with longer follow-up is needed to validate these findings.

Investigative Ophthalmology & Visual Science

Acknowledgments

Disclosure: **A. Belghith**, None; **F.A. Medeiros**, Carl Zeiss Meditec (C, F, R), Heidelberg Engineering (C, F), Topcon (F), Ametek (C, F), Bausch&Lomb (F), Allergan (C, F), Sensimed (F), Alcon (C); **C. Bowd**, None; **J.M. Liebmann**, Alcon (C), Allergan (C), Bausch&Lomb (C, F), Carl Zeiss Meditec (C, F), Diopsys (C, E, F), Heidelberg Engineering (C, F), Merz Pharmaceuticals (C), National Eye Institute (F), New York Glaucoma Research Foundation (F), Optovue (F), Quark Pharmaceuticals (C), Reichert (C, F), Sensimed (C), SOLX (F), Topcon (F), Sustained Nano System (E), Valeant Pharmaceuticals (C), P; **C.A. Girkin**, National Eye Institute (F), EyeSight Foundation of Alabama (F), Research to Prevent Blindness (F), Carl Zeiss Meditec (F), Heidelberg Engineering (F), SOLX (F); **R.N. Weinreb**, Alcon (C), Allergan (C), Ametek (C), Bausch&Lomb (C), Carl Zeiss Meditec (C, F, R), Forsight (C), Genentech (F), Heidelberg Engineering (F), Konan (F), National Eye Institute (F), Neurovision (F), Optovue (F), Quark (F), Reichert (F), Tomey (F), Topcon (C, F), Valeant Pharmaceuticals (C); **L.M. Zangwill**, Carl Zeiss Meditec (F, R), Heidelberg Engineering (F), Optovue (F, R), Topcon (F), Quark (F)

References

1. Varma R, Ying-Lai M, Francis BA, et al.; Los Angeles Latino Eye Study Group. Prevalence of open-angle glaucoma and ocular hypertension in Latinos: the Los Angeles Latino Eye Study. *Ophthalmology*. 2004;111:1439–1448.
2. King AJ, Stead RE, Rotchford AP. Treating patients presenting with advanced glaucoma–should we reconsider current practice? *Br J Ophthalmol*. 2011;95:1185–1192.
3. Leighton P, Lonsdale A, Tildsley J, King A. The willingness of patients presenting with advanced glaucoma to participate in a trial comparing primary medical vs primary surgical treatment. *Eye*. 2012;26:300–306.
4. Traverso C, Walt J, Kelly S, et al. Direct costs of glaucoma and severity of the disease: a multinational long term study of resource utilisation in Europe. *Br J Ophthalmol*. 2005;89:1245–1249.
5. Fiscella RG, Lee J, Davis EJ, Walt J. Cost of illness of glaucoma. *Pharmacoeconomics*. 2009;27:189–198.
6. Lee PP, Walt JG, Doyle JJ, et al. A multicenter, retrospective pilot study of resource use and costs associated with severity of disease in glaucoma. *Arch Ophthalmol*. 2006;124:12–19.
7. Sung KR, Wollstein G, Kim NR, et al. Macular assessment using optical coherence tomography for glaucoma diagnosis. *Br J Ophthalmol*. 2012;96:1452–1455.
8. Sung KR, Sun JH, Na JH, Lee JY, Lee Y. Progression detection capability of macular thickness in advanced glaucomatous eyes. *Ophthalmology*. 2012;119:308–313.
9. Miki A, Medeiros FA, Weinreb RN, et al. Rates of retinal nerve fiber layer thinning in glaucoma suspect eyes. *Ophthalmology*. 2014;121:1350–1358.
10. Lee JM, Cirineo N, Ramanathan M, et al. Performance of the visual field index in glaucoma patients with moderately advanced visual field loss. *Am J Ophthalmol*. 2014;157:39–43.
11. Gardiner SK, Swanson WH, Goren D, Mansberger SL, Demirel S. Assessment of the reliability of standard automated perimetry in regions of glaucomatous damage. *Ophthalmology*. 2014;121:1359–1369.
12. Hood DC, Kardon RH. A framework for comparing structural and functional measures of glaucomatous damage. *Prog Retin Eye Res*. 2007;26:688–710.
13. Mwanza J-C, Budenz DL, Warren JL, et al. Retinal nerve fibre layer thickness floor and corresponding functional loss in glaucoma. *Br J Ophthalmol*. 2015;99:732–737.
14. Mwanza JC, Kim HY, Budenz DL, et al. Residual and dynamic range of retinal nerve fiber layer thickness in glaucoma: comparison of three OCT platforms. *Invest Ophthalmol Vis Sci*. 2015;56:6344–6351.
15. Hood DC, Raza AS, de Moraes CGV, Liebmann JM, Ritch R. Glaucomatous damage of the macula. *Prog Retin Eye Res*. 2013;32:1–21.
16. Saunders LJ, Medeiros FA, Weinreb RN, Zangwill LM. What rates of glaucoma progression are clinically significant? *Exp Rev Ophthalmol*. 2016;11:227–234.
17. Fellman R, Mattox C, Ross K, Vicchrilli S. Know the new glaucoma staging codes. *EyeNet*. 2011;10:65Y6.
18. Belghith A, Bowd C, Medeiros FA, Balasubramanian M, Weinreb RN, Zangwill LM. Learning from healthy and stable eyes: a new approach for detection of glaucomatous progression. *Artif Intell Med*. 2015;64:105–115.
19. Belghith A, Bowd C, Medeiros FA, Balasubramanian M, Weinreb RN, Zangwill LM. Glaucoma progression detection using nonlocal markov random field prior. *J Med Imaging*. 2014;1:034504.
20. Jonas JB, Berenshtein E, Holbach L. Anatomic relationship between lamina cribrosa, intraocular space, and cerebrospinal fluid space. *Invest Ophthalmol Vis Sci*. 2003;44:5189–5195.
21. Downs JC, Roberts MD, Sigal IA. Glaucomatous cupping of the lamina cribrosa: a review of the evidence for active progressive remodeling as a mechanism. *Exp Eye Res*. 2011;93:133–140.
22. Sample PA, Girkin CA, Zangwill LM, et al. The African Descent and Glaucoma Evaluation Study (ADAGES): design and baseline data. *Arch Ophthalmol*. 2009;127:1136–1145.
23. Belghith A, Bowd C, Weinreb RN, Zangwill LM. A hierarchical framework for estimating neuroretinal rim area using 3D spectral domain optical coherence tomography (SD-OCT) optic nerve head (ONH) images of healthy and glaucoma eyes. *Conf Proc IEEE Eng Med Biol Soc*. 2014;2014:3869–3872.
24. Belghith A, Bowd C, Medeiros F, Weinreb R, Zangwill L. Automated segmentation of anterior lamina cribrosa surface: how the lamina cribrosa responds to intraocular pressure change in glaucoma eyes? In: *2015 IEEE 12th International Symposium on Biomedical Imaging (ISBI)*. 2015:222–225.
25. Belghith A, Bowd C, Medeiros FA, et al. Does the location of Bruch's membrane opening change over time? Longitudinal analysis using San Diego Automated Layer Segmentation Algorithm (SALSA) stability of Bruch's membrane opening location over time. *Invest Ophthalmol Vis Sci*. 2016;57:675–682.
26. Rue H, Hurn MA. Bayesian object identification. *Biometrika*. 1999;86:649–660.
27. Belghith A, Collet C, Armspach J. A statistical framework for biomarker analysis and HR-MAS 2D metabolite identification. In: *Computational Surgery and Dual Training*. New York: Springer; 2014:89–112.
28. Kirby M, Miranda R. Circular nodes in neural networks. *Neural Comput*. 1996;8:390–402.
29. Balasubramanian M, Kriegman D, Bowd C, et al. Localized glaucomatous change detection within the proper orthogonal decomposition framework. *Invest Ophthalmol Vis Sci*. 2012;53:3615–3628.
30. Yang H, Qi J, Hardin C, et al. Spectral-domain optical coherence tomography enhanced depth imaging of the normal and glaucomatous nonhuman primate optic nerve head. *Invest Ophthalmol Vis Sci*. 2012;53:394–405.
31. Ye C, Yu M, Leung CK. Impact of segmentation errors and retinal blood vessels on retinal nerve fibre layer measurements using spectral-domain optical coherence tomography. *Acta Ophthalmol*. 2015;94:e211–e219.

Investigative Ophthalmology & Visual Science